LANGMUIR Article
Cite This: Langmuir 2018, 34, 15754−15762
pubs.acs.org/Langmuir

Highly Conductive 2D Metal−Organic Framework Thin Film Fabricated by Liquid−Liquid Interfacial Reaction Using One-Pot-Synthesized Benzenehexathiol

Iu-Fan Chen, Chun-Fu Lu, and Wei-Fang Su*

Department of Materials Science and Engineering, Advanced Research Center of Green Materials Science and Technology, National Taiwan University, Taipei City 10617, Taiwan

Supporting Information

ABSTRACT: Metal−organic frameworks (MOF) are studied extensively in applications like catalysts, gas storage, and sensors due to their various functional groups and structures. Two-dimensional (2D) MOFs such as triphenylene-based materials show excellent charge transport properties, but thin-film fabrication and organic ligand synthesis are difficult. In this work, we synthesize thiol-based organic ligand, benzenehexathiol (BHT), by a simple one-pot reaction. This facile method is safer and faster than conventional synthesis procedure that requires using liquid ammonia as solvent. Two novel 2D MOF materials, Ag_3BHT_2 and Au_3BHT_2, are fabricated by coordinating BHT with either silver (Ag) or gold (Au) ions through liquid−liquid interfacial reaction. The Ag_3BHT_2 thin film reaches a high electrical conductivity of 363 S cm^{-1}, which has potential applications in electronic devices and sensors.

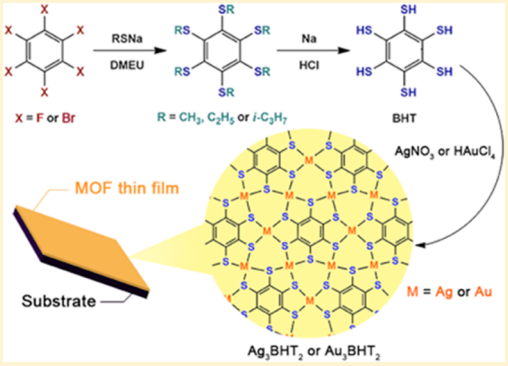

INTRODUCTION

Two-dimensional (2D) materials, like graphene,[1,2] boron nitride,[3] transition-metal dichalcogenides,[4−6] and silicon nanosheets,[7] are widely utilized in electronic and optoelectronic devices, such as transistor, sensor, or electrode. However, these materials are fabricated under high demanding chemical conditions and complicated procedures, so large efforts are dedicated to seek alternating graphene analogous materials. Therefore, 2D metal−organic frameworks (MOF)[8−11] have attracted great research interests recently. Benefiting from their unique chemical, physical, and optoelectronic properties by the planar coordination of metal ions and π-conjugated aromatic organic compounds, 2D MOFs are regarded as one of the potential candidates to replace conventional 2D materials. Additionally, most of them can be prepared through normal chemical procedures with low cost and high yield and offer excellent optoelectronic properties. For example, Sheberla et al.[12] reported devices fabricated by electrically conductive $Ni_3(HITP)_2$ that function as electrochemical double-layer capacitors due to their high conductivity and high surface area. The device can have critical advancement in renewable energy technology. Zhang et al.[13] constructed a new 2D MOF material named NENU-503, which displays high selectivity and recyclable ability as a fluorescent sensor for detecting nitroaromatic explosives.

Among various types of MOFs materials, planar metal bis(dithiolene) complexes have drawn noticeable attention owing to their excellent electronic properties. The five-member ring coordinating by dithiolene with a metal ion provides strong π−d interaction[14] to achieve high electron transfer. Moreover, thiol-based aromatic compounds, including benzenehexathiol (BHT) and triphenylenehexathiol (THT), are highly reactive with metal ions and could easily form ordered planar coordinated structure at room temperature and normal pressure. Huang et al.[15] reported their studies of Cu−BHT, which shows the highest electrical conductivity (1580 S cm^{-1}) in coordination MOF materials reported in the literatures and displays an ambipolar charge-transport behavior. Dong et al.[16] synthesized single-layered conductive THTNi nanosheets that exhibited good performance of electrocatalytic hydrogen production from water. Thus, thiol-based aromatic compounds have been intensively studied in the design and fabrication of novel 2D nanosheets. In general, the thiol-based aromatic compounds are synthesized in anhydrous liquid ammonia as solvent. One must be very careful while using liquid ammonia because the anhydrous ammonia is caustic, corrosive, and harmful when it contacts with human body, especially eyes, lungs, and skin. Incidents with anhydrous ammonia are usually severe because brief exposure to 2500−6500 ppm of anhydrous ammonia can lead to death.[17] Moreover, the synthesis procedure includes several complicated and time-consuming steps at low temperature and in controlled environment. Therefore, a simple and safe method to synthesize thiol-based aromatic compounds is of great interest for further studies and applications in electronics and sensors.

In this work, we successfully developed a novel method to synthesize BHT compound by one-pot reaction without the

Received: November 26, 2018
Published: December 5, 2018

DOI: 10.1021/acs.langmuir.8b03938
Langmuir 2018, 34, 15754−15762

usage of liquid ammonia. The reaction can be completed in 6 h and its yield can reach up to 85%. This approach is not only safer but also simpler than the conventional method to synthesize thiol-based aromatic organic compounds. With an efficient and safe way to synthesize high-purity BHT, 2D MOF materials can be easily developed. We synthesized two new 2D MOFs by coordinating BHT with Ag or Au ions to obtain Ag_3BHT_2 and Au_3BHT_2, respectively. The MOF films were prepared by two different methods. The first one is the direct thin film formation through liquid−liquid interfacial reaction. Two immiscible liquid systems, which dissolve metal-ion salts and BHT respectively, are used as solvents. The thin film would form at their interface. The second one is the pressed thick film from BHT MOF powder, which was synthesized through the direct mixing of metal ion and BHT solutions. The structures and electrical properties of the two films are carefully evaluated. Four-probe measurement indicates that the conductivity of Ag_3BHT_2 can reach 363 S cm^{-1}, which is much higher than most of the reported coordinated polymers[18] and conductive MOF materials.[19−22] The X-ray diffraction (XRD) analysis shows that Ag_3BHT_2 film has a hexagonal lattice structure to obtain a planar conjugation and a $\pi-\pi$ stacking to transport electrons, leading to high electrical conductivity. On the other hand, Au_3BHT_2 is almost insulated because of its disordered structure. Our work provides a more efficient and safer method to synthesize thiol-based aromatic compounds with high reaction yield and purity. Furthermore, we report a brand new, high electrical conductivity 2D MOF material, Ag_3BHT_2, which has potential in applications in electronic devices and sensors.

RESULTS AND DISCUSSION

Synthesis of BHT, Ag_3BHT_2, and Au_3BHT_2. The simple one-pot synthesis method (Scheme 1) is based on two consecutive second-order nucleophilic substitution (S_N2) reactions. The overall reaction consists of three stages. First, the nucleophilic aromatic substitution occurs on hexahalogenobenzene, replacing the halide anions with alkylthiol groups. The procedure is assisted by the high polarity of the solvent 1,3-dimethyl-2-imidazolidinone (DMEU) for a favorable S_N2 reaction. Second, another nucleophilic substitution cleaves the aliphatic groups because of the presence of excess alkylthiolate anions, producing benzenehexathiolate anions. Sodium particles are added into the solution to stabilize the benzenehexathiolate anions. Finally, sodium hexathiolate is treated with hydrochloric acid to obtain benzenehexathiol (BHT). This method provides several advantages: (1) it is simpler, cheaper, and safer than the conventional method to synthesize aromatic thiol-based compounds, which needs the usage of liquid ammonia; (2) using the solvent, excess sodium alkylthiolate and sodium particles can be easily removed by water, leading to high purity; and (3) high reaction yield can be easily achieved because of the one-pot reaction.

Scheme 1. Synthetic Scheme of Benzenehexathiol (BHT) by One-Pot Reaction

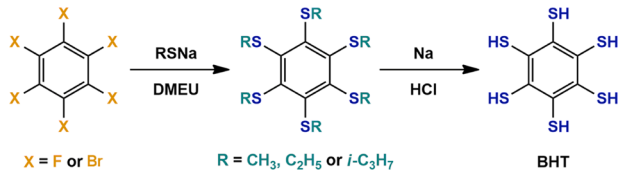

In traditional organic nucleophilic substitution reaction, bromide anion and chloride anion are used extensively as leaving groups due to their electronic stability and the weak carbon−bromide or carbon−chloride bonds. Fluoride anion, on the other hand, is a considerably weaker leaving group than chloride and bromide because carbon−fluorine bond is a strong polar covalent bond. However, fluoride anion can serve as good leaving group in special cases. Testaferri et al.[23] reported the substitution reaction by hexafluorobenzene (C_6F_6) not only has a shorter reaction time but also reacts at lower temperature than hexachlorobenzene (C_6Cl_6) to substitute halide and form hexaalkylthiolbenzene. Fluorine has the highest electron density among all halogen elements, which results in the strong electronic repulsion in a small benzene ring. Therefore, fluoride anion is easier to be substituted than other leaving groups owing to the presence of a strong repulsive force.

To compare the reaction time and reaction yield of different reagents, hexafluorobenzene (C_6F_6) and hexabromobenzene (C_6Br_6) were chosen as starting materials. To achieve a high yield, aliphatic groups must have high efficiency in both nucleophilic substitution reactions. Various alkylthiolate salts, including sodium methylthiolate (CH_3-SNa), sodium ethylthiolate (C_2H_5-SNa), and sodium isopropylthiolate (i-C_3H_7-SNa) were employed to study the effect of an aliphatic group on the reaction. The results are summarized in Table 1, and there are two significant phenomena in these reactions.

Table 1. Synthesis of Benzenehexathiol by Different Starting Materials and Reagents

run	starting material	reagent	temp (°C)	time (h)	yield (%)
1	C_6F_6	CH_3-SNa	0	31	82
2	C_6F_6	C_2H_5-SNa	0	18	81
3	C_6F_6	i-C_3H_7-SNa	0	6	85
4	C_6Br_6	CH_3-SNa	100	72	58
5	C_6Br_6	C_2H_5-SNa	100	56	73
6	C_6Br_6	i-C_3H_7-SNa	100	30	83

First, the reactions employing C_6F_6 as the starting material (runs 1−3) have higher reaction yields and require less reaction time than those using C_6Br_6 (runs 4−6) when the same type of alkylthiolate salt is used. The reactions by C_6Br_6 (runs 4−6) all need to take over 30 h to complete. The first S_N2 substitution on C_6F_6 can occur at 0 °C, whereas the temperature of the reactions of C_6Br_6 occur above 100 °C to replace halide ions. In common organic substitution reaction, fluoride is the weakest leaving group and bromide and chloride are better choices for normal organic synthesis due to their electronic stability. However, our study shows totally contrasting results. With narrow space in an aromatic ring, the fluorides produce a strong electronic repulsion with each other, leading to the easy substitution of fluorides in C_6F_6. Therefore, runs 1−3 with C_6F_6 as the starting material not only possess a higher reaction yield but also can complete at a lower temperature and in a shorter time than runs 4−6, which used C_6Br_6 as the reagent.

Second, the runs with i-C_3H_7-SNa have a much shorter reaction time than those with C_2H_5-SNa and CH_3-SNa. The reaction times of runs with C_2H_5-SNa are shorter than those with CH_3-SNa. Because of both the chain length and spatial

DOI: 10.1021/acs.langmuir.8b03938
Langmuir 2018, 34, 15754−15762

Scheme 2. Formation of Ag_3BHT_2 or Au_3BHT_2

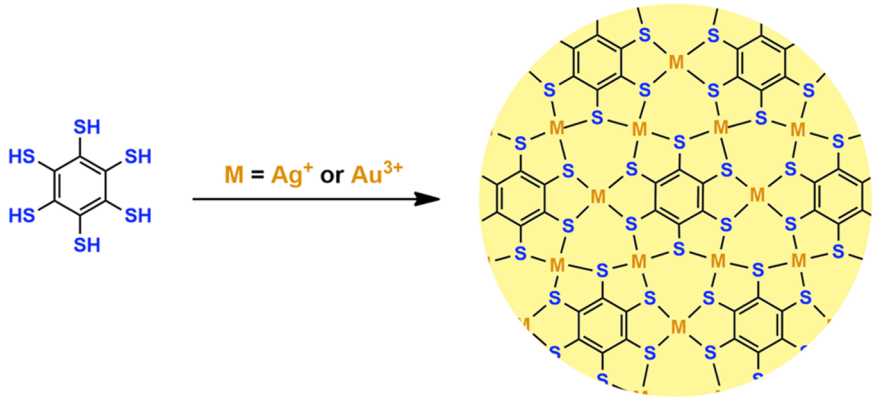

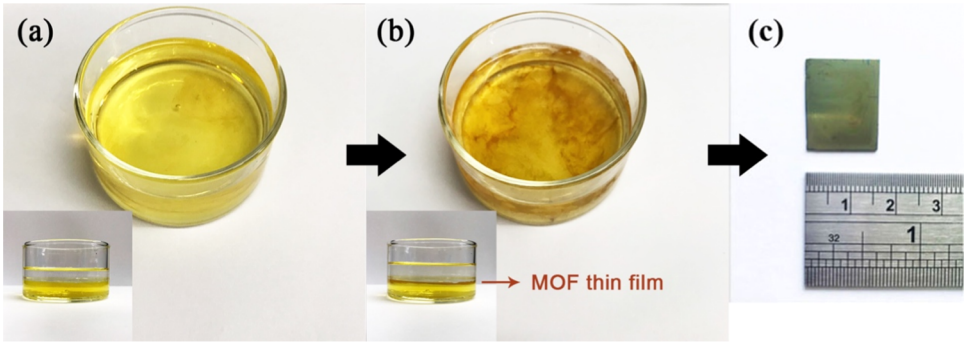

Figure 1. Formation of the Ag_3BHT_2 thin film by liquid−liquid interfacial method. (a) Beginning of the reaction. (b) The formation of the thin film. (c) Film transfer onto the substrate.

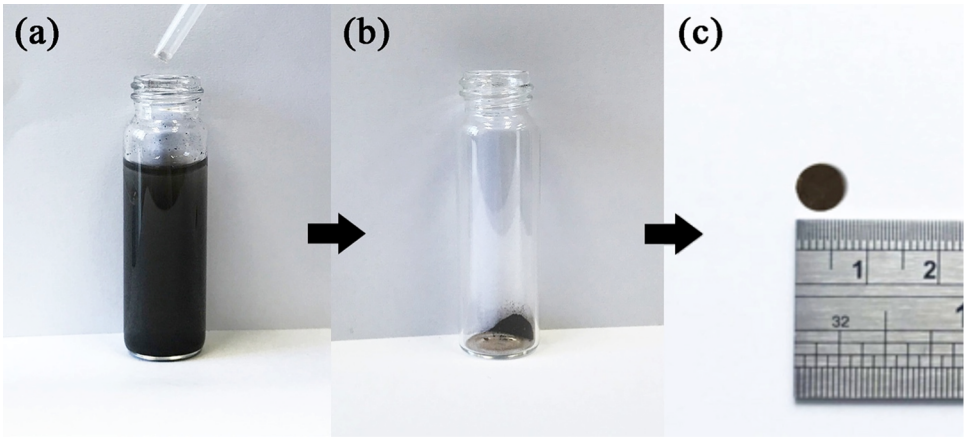

Figure 2. Formation of the Ag_3BHT_2 powder pressed thick film. (a) MOF powder formation by adding metal ion solution into BHT aqueous solution. (b) The Ag_3BHT_2 powder. (c) The powder pressed thick film.

arrangement, the larger aliphatic group exhibits a stronger inductive effect and steric effect than the smaller one. Thus, it makes alkylthiol a stronger nucleophile. The substitution reaction of alkylthiol with the halogenated benzene is easier to take place. The larger the aliphatic group, the shorter the reaction time. The branched chain of isopropyl group can accommodate more negative charge than the linear chain, leading to high stability, so its nucleopholicity is the largest with an abnormally high substitution yield.[24] In Table 1, run 3 has the shortest reaction time (6 h) and the highest reaction yield (85%), with C_6F_6 and *i*-C_3H_7-SNa as starting materials. Run 2 (C_6F_6 and C_2H_5-SNa) has a similar yield as run 1 (C_6F_6 and CH_3-SNa) but a shorter reaction time (18 h) than the latter (31 h). The similar trend is also observed in runs 4−6. Run 6 (C_6Br_6 and *i*-C_3H_7-SNa) has the second highest reaction yield among all runs, confirming the excellent nucleophilic characteristic of isopropyl groups. Run 4, with C_6Br_6 and CH_3-SNa, has the longest reaction time (72 h) and the lowest reaction yield (58%) among all the reactions, corresponding to the poor leaving ability of bromide ion in the first S_N2 reaction and weak inductive effect and steric effect of methyl groups in both reactions. To sum up, we obtain an efficient, simple, and rapid method to synthesize BHT by using C_6F_6 and *i*-C_3H_7-SNa as the starting material, and the reaction has a yield of 85% in 6 h.

DOI: 10.1021/acs.langmuir.8b03938
Langmuir 2018, 34, 15754−15762

Being highly reactive with metal ions, BHT can easily coordinate with Ag or Au ions. The MOF can be obtained by direct interaction between BHT and metal ions (Scheme 2). One BHT molecule can coordinate with six metal ions, composing a 6-fold symmetric 2D planar structure. The films of BHT-based MOF was prepared by two methods: (1) thin film: direct film formation through liquid−liquid interfacial reaction (Figure 1) and (2) thick film: pressed film from BHT MOF powder (Figure 2). The thick films were used to perform the analysis of Fourier transform infrared spectrometer (FT-IR). Both thin films and thick films were used to characterize the bonding by X-ray photoelectron spectroscopy (XPS), crystallinity by X-ray diffraction (XRD) analysis, and conductivity of the materials by four-point probe. The detailed procedure is described in the section of Experimental Methods. The reaction time of Ag_3BHT_2 is shorter than that of Au_3BHT_2 for both thin film and powder. The formation of Ag_3BHT_2 thin film can be observed by naked eyes in 30 min at the liquid interface, whereas Au_3BHT_2 thin film needs 6.5 h to reach the thickness to be seen by naked eye. The concentration of both metal ion and BHT solution should be carefully controlled. When a concentration of precursor higher than 0.1% is used, the thin film at the liquid interface would be too thick to sustain and collapse. The MOF thin film could not be seen if the concentration of the solution is lower than 0.015%. Ag_3BHT_2 powder is precipitated immediately after mixing the BHT and $AgNO_3$ aqueous solution; however, the synthesis of Au_3BHT_2 by BHT and $HAuCl_4$ solution needs to be heated at 50 °C for 30 min. The shorter reaction time of Ag_3BHT_2 is due to the higher reactivity of Ag ions than that of Au ions.[25]

Materials Characterization. To determine the bonding between metal ions and BHT, FT-IR was employed to study BHT, using thick films of Ag_3BHT_2 and Au_3BHT_2 for high absorption intensity. In Figure 3, the FT-IR of BHT has a peak

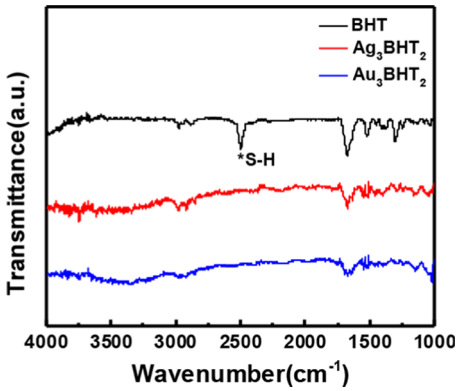

Figure 3. FT-IR spectra of BHT powder (black), the Ag_3BHT_2 thick film (red), and the Au_3BHT_2 (blue) thick film.

at 2500 cm^{-1}, which corresponds to the sulfur−hydrogen bond, whereas Ag_3BHT_2 and Au_3BHT_2 show no absorption at the same range. The difference means that the hydrogen atoms on BHT were removed to coordinate with metal ions.

The chemical states of metal ions and sulfur in MOFs were determined by XPS. In Figure 4a, the peak of Ag $3d_{3/2}$ at 367.5 eV corresponds to Ag(I) in the Ag_3BHT_2 thin film. The measured binding energy differs from that of unbonded Ag (368.3 eV),[26] confirming the coordination bonding of silver ions and sulfur ions. Figure 4b shows S $2p_{3/2}$ and $2p_{1/2}$ peaks at 161.9 and 163.1 eV, indicating the sulfur ions bond with metal ions.[27] Thus, the coordination between Ag and BHT is well defined in the Ag_3BHT_2 thin film. In Figure 4c, the binding energy of Au has two peaks at 84.9 and 88.6 eV, which matches to Au(I) $4f_{7/2}$ and $4f_{5/2}$ respectively.[27] The result points out that Au(III) ions have been reduced when they coordinated to BHT. Figure 4d also shows the binding energy of S $2p_{3/2}$ and $2p_{1/2}$ representing the coordination by BHT and Au ions.

It is worth mentioning that the XPS results of MOF thick films (Figure 5) show interesting differences from those of MOF thin films. First, in Figure 5a, the peak of Ag $3d_{3/2}$ of the Ag_3BHT_2 thick film is similar to that of the Ag_3BHT_2 thin film. However, in Figure 5b, different from the result of the thin film, there are unreacted thiols (−SH, 162.5 and 163.6 eV) and unbonded sulfur ions ($-S^-$, 163.9 and 165.0 eV) remaining in the Ag_3BHT_2 thick film. The existence of unbonded sulfur ions and unreacted thiols in the Ag_3BHT_2 thick film indicates an incomplete coordination between BHT and Ag ions because of the rapid formation. In Figure 5c, the XPS result of Au of the Au_3BHT_2 thick film states that Au has two oxidation states. The four peaks correspond to Au(I) $4f_{7/2}$, $4f_{5/2}$ and Au(0) $4f_{7/2}$, $4f_{5/2}$ (85.9 and 89.4 eV, respectively), which means that the gold ions have different chemical states in the Au_3BHT_2 thick film. In Figure 5d, the peaks of sulfur indicate that the signals of unreacted thiols can also be observed. The results of unreacted BHT and the multivalent Au ions in the Au_3BHT_2 thick film mean that the coordination of BHT and Au ions is incomplete. Compared with the Ag_3BHT_2 thick film, there are no signals of unbonded sulfur ions in the Au_3BHT_2 thick film. Because of the long reaction time, the sulfur ions might be all consumed by metal ions, leaving no unbonded sulfur ions signal. It is noted that although unreacted thiols are observed in the XPS spectra, no absorption signals of the thiol groups are detected by FT-IR spectroscopy. This is due to the low concentration of unreacted thiols, which is below the detection limit of FT-IR. Also, the XPS signals come from the surface of the materials, where the concentration of defects and unreacted ligands are higher than that in the bulk material.

The electrical conductivities of all the thin films and thick films of Ag_3BHT_2 and Au_3BHT_2 were measured by the four-point probe method. The thickness of the film was determined from the cross-sectional scanning electron microscopy (SEM) image of the samples (Figures S5 and S6). The results are summarized in Table 2. A $I-V$ curve of the measurements is included in Figure S1 in the Supporting Information. For the Ag_3BHT_2 thin film, the conductivity can reach up to 363 S cm^{-1}. Huang et al.[15,28] reported the Cu−BHT film with a record conductivity of 1580 S cm^{-1} in 2015, and their parallel work of Ag−BHT film was published recently with a conductivity of 250 S cm^{-1}. Kambe et al.[29] reported the $Ni_3(BHT)_2$ in 2014, which has a conductivity of 160 S cm^{-1}; in 2016, the $Ni_3(HITP)_2$ material reported by Sheberla et al.[12] possesses the conductivity of 40 S cm^{-1}. No other conductive MOF materials reported to date could reach over 10 S cm^{-1}. The Ag_3BHT_2 thin film in this work displays an impressive high conductivity among the conductive MOF materials. The conductivity could be partly contributed to the strong π−d conjugation between sulfur ions and silver ions.[14] Furthermore, the ordered crystal structure of Ag_3BHT_2 can introduce excellent $\pi-\pi$ stacking effect in the interlayer direction for high charge transport. From the XRD patterns (Figure 6), the Ag_3BHT_2 thin film has an ordered hexagonal planar structure, leading to the superb intralayer and interlayer charge transport ability. For the Ag_3BHT_2 thick film, the conductivity is 19.8 S

DOI: 10.1021/acs.langmuir.8b03938
Langmuir 2018, 34, 15754−15762

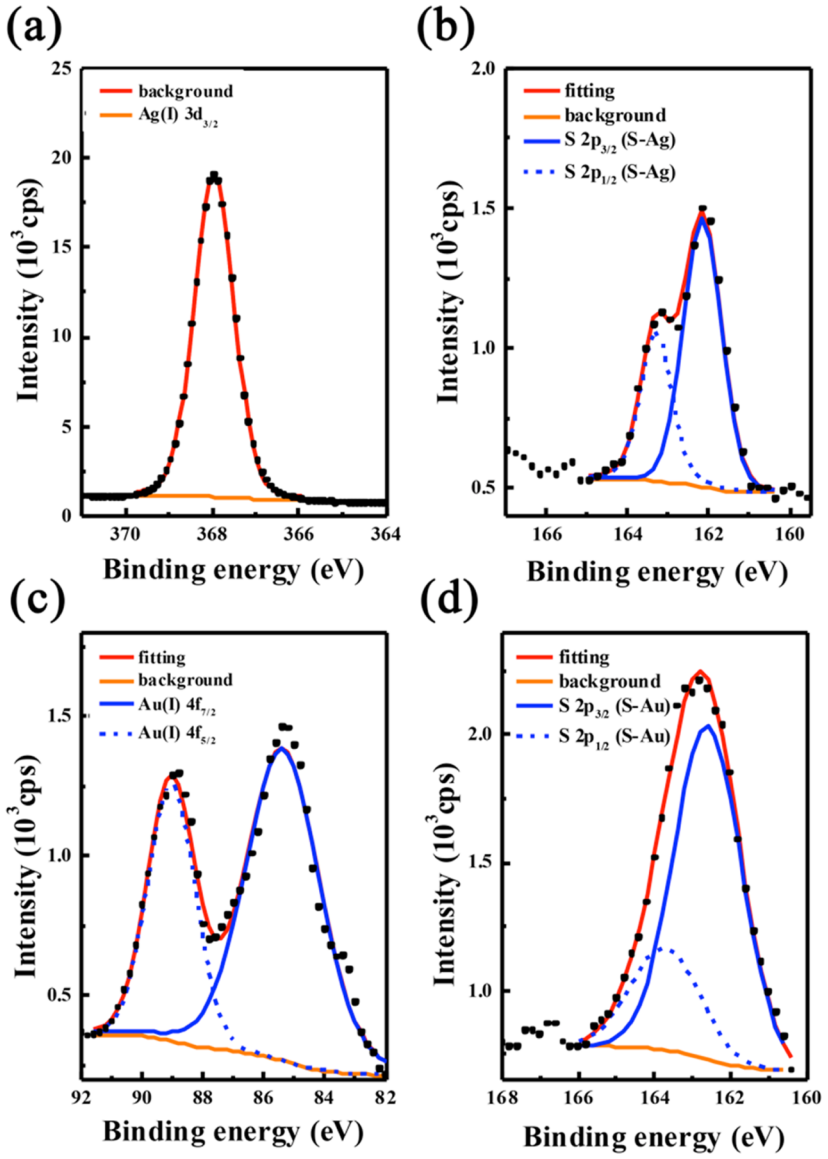

Figure 4. XPS spectra of (a) Ag $3d_{3/2}$ and (b) S $2p_{1/2}$, $2p_{3/2}$ in the Ag_3BHT_2 thin film, (c) Au $4f_{5/2}$, $4f_{7/2}$, and (d) S $2p_{1/2}$, $2p_{3/2}$ in the Au_3BHT_2 thin film.

cm^{-1}, lower than that of the thin film. The difference in the conductivity between the thin film and the thick film might be caused by crystallinity[30] and the presence of unreacted BHT. The thick film of Ag_3BHT_2 has a weaker XRD intensity than the thin film, showing the less ordered structure of thick film than that of the thin film. Because the electrical conductivity results from the delocalized electron transfer through the conjugated planar structure and the $\pi-\pi$ stacking from layer to layer, the thick film pressed from random orientation powder is expected to have a lower conductivity than the thin film. The XPS analysis shows that some BHT molecules are not fully coordinated with silver ions in the Ag_3BHT_2 thick film as discussed before. Therefore, the packing of MOF thick film is less ordered and looser than that of MOF thin film. A more ordered thin film is expected to have a higher conductivity than a thick film.

For Au_3BHT_2, however, both the thin film and thick film exhibit low conductivity. The large discrepancy in Au_3BHT_2 might be due to its disrupted structure. The lattice structures of Ag_3BHT_2 and Au_3BHT_2 are speculated to be 2D planar hexagonal coordinated polymer, with one BHT molecule connected to six metal ions and each metal ion coordinated with four sulfurs. The XRD analysis has shown the structural difference between the thin films of Ag_3BHT_2 and Au_3BHT_2. To characterize the MOF thin film, out-of-plane diffraction was employed. For Ag_3BHT_2, the out-of-plane diffraction patterns shows the peak of (001) at 29.19°, which indicates the interlayer distance of 3.06 Å. Moreover, the peaks at 9.48, 16.45, and 19.02° correspond to the (100), $(2\bar{1}0)$, and (200) of a hexagonal lattice structure with lattice constant $a = b =$ 10.77 Å. The large full width at half-maximum of the diffraction peaks indicates the Ag_3BHT_2 thin film comprises small crystal grains. Also, these crystals are polycrystalline because the in-plane peaks, (100), $(2\bar{1}0)$, and (200), are observed in the out-of-plane XRD patterns. (Simulation of XRD patterns also confirmed the hexagonal structure of Ag_3BHT_2.) The XRD patterns of Au_3BHT_2 thin film also display (100) and (001) at the same angle as Ag_3BHT_2; however, the weak intensity of the peaks and the lack of order diffraction signals indicate that the Au_3BHT_2 thin film has a

DOI: 10.1021/acs.langmuir.8b03938
Langmuir 2018, 34, 15754−15762

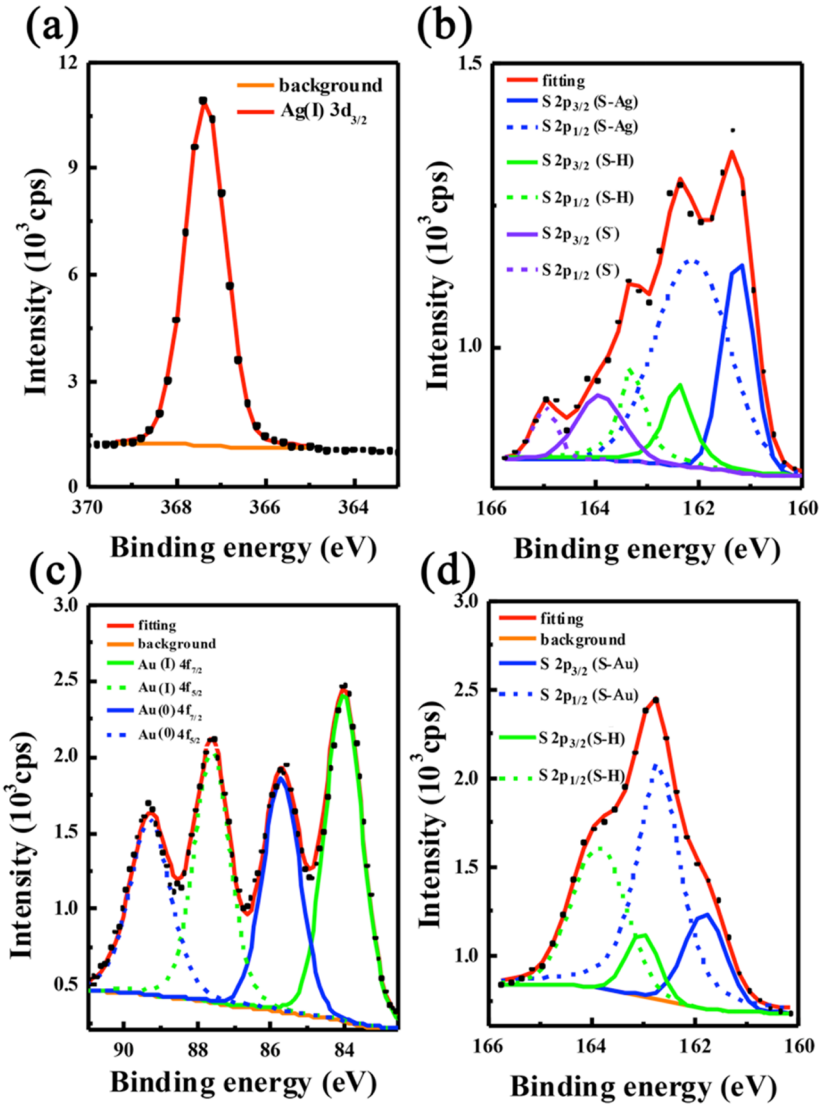

Figure 5. XPS spectra of (a) Ag $3d_{3/2}$ and (b) S $2p_{1/2}$, $2p_{3/2}$ in the Ag_3BHT_2 thick film and (c) Au $4f_{5/2}$, $4f_{7/2}$ and (d) S $2p_{1/2}$, $2p_{3/2}$ in the Au_3BHT_2 thick film.

Table 2. Thickness and Conductivity of BHT-MOFs

sample	thickness	conductivity (S cm^{-1})
Ag_3BHT_2 thin film	276.51 ± 5.53 nm	290 ± 23.2 (363)
Ag_3BHT_2 thick film	64.23 ± 0.43 μm	14.2 ± 3.0 (19.8)
Au_3BHT_2 thin film	324.72 ± 11.23 nm	9.15 ± 0.21 × 10^{-5} (1.12 × 10^{-4})
Au_3BHT_2 thick film	89.05 ± 0.12 μm	7.46 ± 1.12 × 10^{-5} (8.07 × 10^{-5})

lower crystallinity than Ag_3BHT_2. The Au_3BHT_2 thin film might be distorted and deviated from planer structure; that is, the two BHT molecules bonded with an Au ion are not placed on a same plane, which would cause random orientation and loose packing of the structure. Without an ordered planar structure, charge transport in Au_3BHT_2 is interrupted in both planar and interlayer directions, leading to insulation property. For the Ag_3BHT_2 and Au_3BHT_2 thick films, the XRD patterns are extremely weak, showing that both samples have low crystallinity (Figure S2).

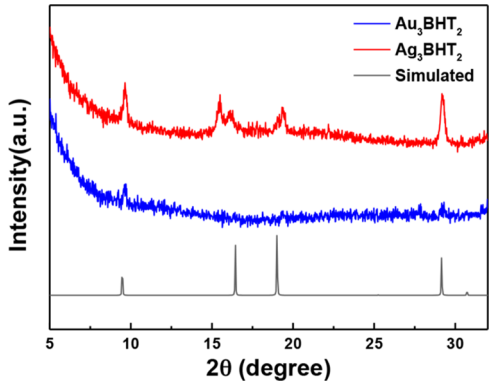

Figure 6. XRD patterns of Ag_3BHT_2 thin film (red), Au_3BHT_2 thin film (blue), and stimulated result (gray).

Morphological differences between the thick films and the thin films of Ag_3BHT_2 and Au_3BHT_2 are shown by scanning electron microscopy (SEM) images (Figure 7). The thin film of Ag_3BHT_2 is flat (Figure 7a) but has cracks and small particles on the surface, whereas the Au_3BHT_2 thin film

DOI: 10.1021/acs.langmuir.8b03938
Langmuir 2018, 34, 15754−15762

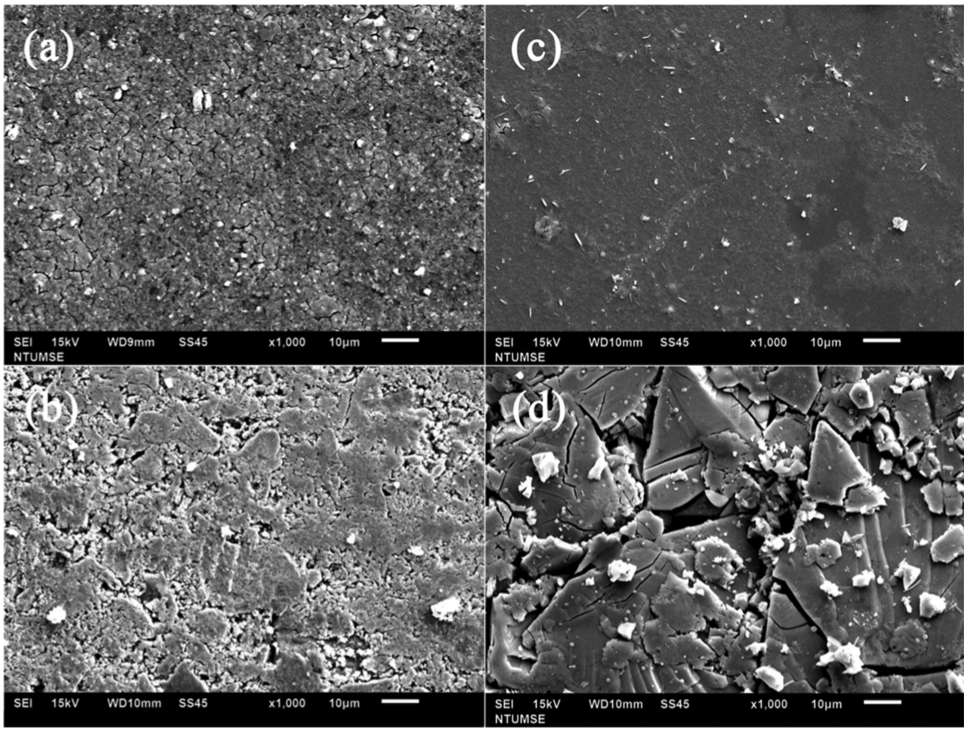

Figure 7. SEM images of the Ag_3BHT_2 (a) thin film and (b) thick film and the Au_3BHT_2 (c) thin film and (d) thick film.

(Figure 7c) is extremely uniform without any micrometer-scaled pores in the film. The morphology of the Ag_3BHT_2 powder pressed thick film has a larger roughness than the thin film, but still is a large-scale continuous structure (Figure 7b). Figure 7d shows that the Au_3BHT_2 thick film is cracked and discontinuous, with large variation in the sizes of the domain from 10 to 100 μm. The differences in the morphology between the thin films of Ag_3BHT_2 and Au_3BHT_2 might result from the different reaction rate. The slower reaction rate of the Au_3BHT_2 thin film formation resulted in the smooth film. The MOF thin films have less cracks and coarseness than powder pressed thick films, resulting in a long-range continuous morphology. Despite the small discontinuous cracks on the surface of the Ag_3BHT_2 thin film and thick film, both reach the threshold of the percolation network, exhibiting a high electrical conductivity. The morphologies of the Au_3BHT_2 thin film and thick film have similar trend as Ag_3BHT_2. The morphological difference between the MOF thin films and powder pressed thick film in SEM images are agreed with the results of XRD study.

Ag_3BHT_2 has a higher electrical conductivity than Au_3BHT_2 because of a strong π–d interaction and π–π stacking via the hexagonal planar conjugated structure, which is determined by the XRD analysis. In the aspect of morphology, the MOF thin films exhibit a highly ordered and long-range continuous orientation, leading to a higher conductivity than MOF powder pressed thick films, which have incomplete coordination and disordered morphology. Hence, the conductivity of Ag_3BHT_2 can be increased by improving the microstructure through liquid–liquid interfacial method to reach up to 363 S cm^{-1}.

CONCLUSIONS

In this work, we demonstrated a brand new approach to synthesize BHT by a simple one-pot reaction without using liquid ammonia. The reaction of starting materials as hexafluorobenzene and sodium isopropylthiolate can be completed in only 6 h and achieve a yield of 85%. This method provides a safer and easier way to synthesize thiol-based aromatic compounds. With four-point probe measurement, the electrical conductivity of the Ag_3BHT_2 thin film can reach 363 S cm^{-1}, which is much higher than that of most conductive coordination polymers. The differences between Ag_3BHT_2 and Au_3BHT_2 were investigated; the Ag_3BHT_2 thin film has a hexagonal lattice planar structure, but the structure of the Au_3BHT_2 thin film is disordered. Au_3BHT_2 is almost insulated because of its random orientation that lacks planar conjugation and π–π stacking to transport electrons. With large-scale continuous crystalline morphology and complete coordination by BHT and Ag ions, the Ag_3BHT_2 thin film fabricated by liquid–liquid interfacial method exhibits a higher electrical conductivity than powder pressed thick film. With a high conductivity and a simple synthesis procedure, Ag_3BHT_2 is a potential material to be utilized in the applications of electronic devices and sensors.

EXPERIMENTAL METHODS

Synthesis of Benzenehexathiol (BHT). The solution of hexahalogenobenzene (14 mmol) and sodium alkylthiolate (0.21 mol) with 1,3-dimethyl-2-imidazolidinone (DMEU, 30 mL) was stirred under nitrogen at either 0 or 100 °C. The progress of the reaction was monitored by thin layer chromatography (TLC). Hexahalogenobenzene was converted into hexaalkylthiolbenzene after complete reaction. Sodium particles (0.644 g, 28 mmol) were added, and the solution was heated to 100 °C. The reaction was monitored by TLC. Methanol (30 mL) and water (30 mL) were injected into the flask, respectively, and the solution was poured into hydrochloric acid (1.0 M, 150 mL) slowly. The yellow solid (3.215 g, 85%) was then precipitated, filtered, and washed with water (20 mL*3) and acetone (20 mL*3). ^{1}H NMR (NMR, Figure S3) (400 MHz, CD3CN): δ (ppm) 2.09 (s, 6H). Electrospray ionization mass spectroscopy (ESI-MS, Figure S4): $[M + 2H]^{2+}$: 137.07. Calculated for $C_6S_6H_6$: 270.47 (mg/mol). Found: 272.13 (mg/mol).

DOI: 10.1021/acs.langmuir.8b03938
Langmuir 2018, 34, 15754–15762

Formation of Ag_3BHT_2 and Au_3BHT_2. The MOF thin film was prepared by liquid−liquid interfacial reaction. BHT (5 mg, 0.0185 mmol) was first dissolved in sodium hydroxide aqueous solution (5 mM, 10 mL), and the solution was added into a round dish (with 30 mm diameter). $AgNO_3/HAuCl_4$ (0.025 mmol) was dissolved in the co-solvent of acetonitrile and ethyl acetate (v/v = 1:4, 10 mL). Then, clean acetonitrile/ethyl acetate co-solvent (5 mL) was added to cover the aqueous layer, forming an organic−aqueous interface. After that, the metal-ion solution was gently injected into the upper layer using a syringe. The brown MOF thin film was formed at the liquid−liquid interface and can be observed through eyes. The Ag_3BHT_2 film was formed in 30 min, whereas the formation of the Au_3BHT_2 film took 6.5 h. The silicon wafer covered with 300 nm silicon oxide was placed in the dish in advance, and the liquid was removed by syringe slowly to deposit the MOF thin film on the substrate. The MOF powder was obtained by mixing BHT (10 mg, 0.037 mmol) and $AgNO_3/HAuCl_4$ (0.1 mmol) in methanol (30 mL) directly, and small MOF particles were precipitated. Ag_3BHT_2 particles can form immediately, and the precipitation of Au_3BHT_2 needs to heat the solution to 50 °C for 30 min. The particles were filtered, washed with water and acetone in sequence, dried by vacuum, and pressed into a disk in a mold under a pressure of 50 psi (with a diameter of 7 mm). Elemental analysis was done by energy-dispersive X-ray spectroscopy (EDS), which identifies the elements present and atomic percentage (Tables S1 and S2).

Materials Characterization. The MOF thin films were deposited on 20 × 20 mm^2 silicon substrates with 300 nm thermally grown SiO_2. The powder was pressed into a die to form thick film with a diameter of 7 mm. The sheet resistance was measured by four-point probe and Keithley 2400 equipped with Labview software using current from 10 to 20 mA. ^1H NMR spectrum of BHT was performed by A525-Bruker AVIII HD 400 MHz NMR with *d*-acetonitrile (CD_3CN) as *d*-solvent, and ESI-MS was made by FINNIGAN LCQ Mass Spectrometry, with BHT dissolved in 20 mL dichloromethane (0.56 mM). FT-IR spectra of BHT, thick film of Ag_3BHT_2 and Au_3BHT_2 were acquired by PerkinElmer Spectrum 100 FT-IR Spectrometer. The out-of-plane XRD patterns of the MOF films of Ag_3BHT_2 and Au_3BHT_2 were measured by Rigaku TTRAX3 X-ray diffraction analyzer (15 kW, λ = 1.541 Å) from 2θ = 5 to 35°. The simulations of diffraction patterns were calculated by Materials Studio 8.0 software. The thickness of the thin film and the thick film was determined from the SEM cross-sectional images of the samples (Figures S5 and S6). The SEM surface images and the EDS of the films and the cross-sectional images of the thick films were taken by JEOL JSM6510 scanning electron microscopy at 15 and 10 kV, respectively. The SEM cross-sectional images of the thin films were taken by NOVA NANO SEM 450. The samples for the SEM and EDS were first covered with platinum with the thickness of 5 nm. The PHI 5000 Versa Probe system (ULVAC-PHI, Chigasaki) with a microfocused (100 μm) Al X-ray beam was used to obtain the XPS spectra of the Ag_3BHT_2 and Au_3BHT_2 films.

■ ASSOCIATED CONTENT

Supporting Information

The Supporting Information is available free of charge on the ACS Publications website at DOI: 10.1021/acs.langmuir.8b03938.

Conductivity measurement of the Ag_3BHT_2 thin film; XRD results of the MOF thick film; ^1H NMR and ESI-MS analyses of BHT; the SEM images of cross-sectional of both thin and thick films; elemental analysis of the Ag_3BHT_2 and Au_3BHT_2 thin films (PDF)

■ AUTHOR INFORMATION

Corresponding Author

*E-mail: suwf@ntu.edu.tw.

ORCID

Wei-Fang Su: 0000-0002-3375-4664

Author Contributions

The manuscript was written through contributions of all the authors. All the authors have given approval to the final version of the manuscript.

Funding

This work was financially supported by the "Advanced Research Center of Green Materials Science and Technology" from The Featured Area Research Center Program within the framework of the Higher Education Sprout Project by the Ministry of Education (107L9006) and the Ministry of Science and Technology in Taiwan (MOST 106-2218-E-002-021-MY2 and 107-3017-F-002-001). The authors also thank the partial financial support from the grant of MOST 106-2923-M-002-004-MY3.

Notes

The authors declare no competing financial interest.

■ ACKNOWLEDGMENTS

Authors also thanks the technical supports provided by Chien-An Chen (synthesis), Tzu-Yi Yu (NMR), Bo-Chang Lai, Sze-Yin Lin, Yu-Tao Sun (thickness measurement), and Instrumental Center of National Taiwan University (ESI-MS, FINNIGAN LCQ Mass Spectrometry).

■ REFERENCES

(1) Geim, A. K.; Novoselov, K. S. The rise of graphene. *Nat. Mater.* **2007**, *6*, 183−191.

(2) Geim, A. K. Graphene: Status and Prospects. *Science* **2009**, *324*, 1530−1534.

(3) Song, L.; Ci, L.; Lu, H.; Sorokin, P. B.; Jin, C.; Ni, J.; Kvashnin, A. G.; Kvashnin, D. G.; Lou, J.; Yakobson, B. I.; Ajayan, P. M. Large scale growth and characterization of atomic hexagonal boron nitride layers. *Nano Lett.* **2010**, *10*, 3209−3215.

(4) Mak, K. F.; Lee, C.; Hone, J.; Shan, J.; Heinz1, T. F. Atomically thin MoS_2: a new direct-gap semiconductor. *Phys. Rev. Lett.* **2010**, *105*, No. 136805.

(5) Manzeli, S.; Ovchinnikov, D.; Pasquier, D.; Yazyev, O. V.; Kis, A. 2D transition metal dichalcogenides. *Nat. Rev. Mater.* **2017**, *2*, No. 17033.

(6) Wang, Q. H.; Kalantar-Zadeh, K.; Kis, A.; Coleman, J. N.; Strano, M. S. Electronics and optoelectronics of two-dimensional transition metal dichalcogenides. *Nat. Nanotechnol.* **2012**, *7*, 699−712.

(7) Okamoto, H.; Kumai, Y.; Sugiyama, Y.; Mitsuoka, T.; Nakanishi, K.; Ohta, T.; Nozaki, H.; Yamaguchi, S.; Shirai, S.; Nakano, H. Silicon nanosheets and their self-assembled regular stacking structure. *J. Am. Chem. Soc.* **2010**, *132*, 2710−2718.

(8) Ko, M.; Mendeckia, L.; Mirica, K. A. Conductive two-dimensional metal-organic frameworks as multifunctional materials. *Chem. Commun.* **2018**, *54*, 7873−7891.

(9) Furukawa, H.; Cordova, K. E.; OKeeffe, M.; Yaghi, O. M. The chemistry and applications of metal-organic frameworks. *Science* **2013**, *341*, No. 1230444.

(10) Kuppler, R. J.; Timmons, D. J.; Fang, Q.-R.; Li, J.-R.; Makal, T. A.; Young, M. D.; Yuan, D.; Zhao, D.; Zhuang, W.; Zhou, H.-C. Potential applications of metal-organic frameworks. *Coordin. Chem. Rev.* **2009**, *253*, 3042−3066.

(11) Zhou, H. C.; Kitagawa, S. Metal-organic frameworks (MOFs). *Chem. Soc. Rev.* **2014**, *43*, 5145−5148.

(12) Sheberla, D.; Bachman, J. C.; Elias, J. S.; Sun, C.-J.; Shao-Horn, Y.; Dinca, M. Conductive MOF electrodes for stable supercapacitors with high areal capacitance. *Nat. Mater.* **2016**, *16*, 220−224.

(13) Zhang, S. R.; Du, D. Y.; Qin, J. S.; Bao, S.-J.; Li, S.-L.; He, W.-W.; Lan, Y.-Q.; Shen, P.; Su, Z.-M. A fluorescent sensor for highly selective detection of nitroaromatic explosives based on a 2D, extremely stable, metal-organic framework. *Chem. - Eur. J.* **2014**, *20*, 3589−3594.

DOI: 10.1021/acs.langmuir.8b03938
Langmuir 2018, 34, 15754−15762

(14) Hendon, C. H.; Tianaa, D.; Walsh, A. Conductive metal-organic frameworks and networks: fact or fantasy? *Phys. Chem. Chem. Phys.* **2012**, *14*, 13120−13132.
(15) Huang, X.; Sheng, P.; Tu, Z.; Zhang, F.; Wang, J.; Geng, H.; Zou, Y.; Di, C. A.; Yi, Y.; Sun, Y.; Xu, W.; Zhu, D. A. A two-dimensional pi-d conjugated coordination polymer with extremely high electrical conductivity and ambipolar transport behaviour. *Nat. Commun.* **2015**, *6*, No. 7408.
(16) Dong, R.; Pfeffermann, M.; Liang, H.; Zheng, Z.; Zhu, X.; Zhang, J.; Feng, X. Large-Area, free-Standing, two-dimensional supramolecular polymer single-layer sheets for highly efficient electrocatalytic hydrogen evolution. *Angew. Chem., Int. Ed.* **2015**, *54*, 12058−12063.
(17) Ammonia Solution (UN 3318); Ammonia Anhydrous (UN 1005). The National Institute for Occupational Safety and Health, Emergency Response Safety and Health Database. https://www.cdc.gov/niosh/ershdb/emergencyresponsecard_29750013.html (accessed May 24, 2018).
(18) Givaja, G.; Amo-Ochoa, P.; Gómez-García, C. J.; Zamora, F. Electrical conductive coordination polymers. *Chem. Soc. Rev.* **2012**, *41*, 115−147.
(19) Sun, L.; Campbell, M. G.; Dinca, M. Electrically conductive porous metal-organic frameworks. *Angew. Chem., Int. Ed.* **2016**, *55*, 3566−3579.
(20) Sadakiyo, M.; Yamada, T.; Kitagawa, H. Rational designs for highly proton-conductive metal-organic frameworks. *J. Am. Chem. Soc.* **2009**, *131*, 9906−9907.
(21) Wu, G.; Huang, J.; Zang, Y.; He, J.; Xu, G. Porous field-effect transistors based on a semiconductive metal-organic framework. *J. Am. Chem. Soc.* **2017**, *139*, 1360−1363.
(22) Jia, H.; Yao, Y.; Zhao, J.; Gao, Y.; Luo, Z.; Du, P. A novel two-dimensional nickel phthalocyanine-based metal-organic framework for highly efficient water oxidation catalysis. *J. Mater. Chem. A* **2018**, *6*, 1188−1195.
(23) Testaferri, L.; Tingoli, M.; Tiecco, M. Reactions of polychlorobenzenes with alkanethiol anions in HMPA. A simple, high-yield synthesis of poly(alkylthio)benzenes. *J. Org. Chem.* **1980**, *45*, 4376−4380.
(24) Smith, R. P.; Eyring, H. The inductive effect and chemical reactivity. III. Effect of charge shifts on energetics of some basic reactions of aliphatic compounds. *J. Am. Chem. Soc.* **1953**, *75*, 5183−5186.
(25) Bartlett, N. Relativistic effects and the chemistry of gold. *Gold Bull.* **1998**, *31*, 22−25.
(26) Gaarenstroom, S. W.; Winograd, N. Initial and final state effects in the ESCA spectra of cadmium and silver oxides. *J. Chem. Phys.* **1977**, *67*, 3500−3506.
(27) Castner, D. G.; Hinds, K.; Grainger, D. W. X-ray photoelectron spectroscopy sulfur 2p study of organic thiol and disulfide binding interactions with gold surfaces. *Langmuir* **1996**, *12*, 5083−5086.
(28) Huang, X.; Li, H.; Tu, Z.; Liu, L.; Wu, X.; Chen, J.; Liang, Y.; Zou, Y.; Yi, Y.; Sun, J.; Xu, W.; Zhu, D. Highly conducting neutral coordination polymer with infinite two-dimensional silver−sulfur networks. *J. Am. Chem. Soc.* **2018**, *140*, 15153−15156.
(29) Kambe, T.; Sakamoto, R.; Kusamoto, T.; Pal, T.; Fukui, N.; Hoshiko, K.; Shimojima, T.; Wang, Z.; Hirahara, T.; Ishizaka, K.; Hasegawa, S.; Liu, F.; Nishihara, H. Redox control and high conductivity of nickel bis(dithiolene) complex π-nanosheet: A potential organic two-dimensional topological insulator. *J. Am. Chem. Soc.* **2014**, *136*, 14357−14360.
(30) Huang, X.; Yao, H.; Cui, Y.; Hao, W.; Zhu, J.; Xu, W.; Zhu, D. Conductive copper benzenehexathiol coordination polymer as a hydrogen evolution catalyst. *ACS Appl. Mater. Interfaces* **2017**, *9*, 40752−40759.

DOI: 10.1021/acs.langmuir.8b03938
Langmuir 2018, 34, 15754−15762